The Effects of Induced B_0 and B_1 Magnetic Field Perturbations on Efforts to Image Near Embedded Metal Hardware

K. M. Koch[1], K. F. King[1], and G. C. McKinnon[1]
[1]Applied Science Laboratory, GE Healthcare, Waukesha, WI, United States

Introduction: Recent developments have enabled spatially accurate MR imaging near embedded metal hardware. Both the MAVRIC [1,2] and SEPI-VAT [3] techniques apply alternative imaging strategies that effectively divide large spectral dispersions near metal implants (~20 kHz) into manageable and separately imaged spectral bins. Both of these techniques have shown great promise in acquiring high-resolution images in the direct vicinity of metal implants within clinically viable scan times using conventional clinical MR hardware. Here, we describe the remaining challenges and limitations when using these new techniques to image near metal implants. The primary remaining challenges are: (a) applying Fourier-based frequency encoding processes in the presence of perturbing local B_0 field gradients of the same order of magnitude of the encoding gradient and (b) perturbations to the B_1 magnetic field induced by the embedded metal hardware.

Methods: The effects of local B_0 gradients and B_1 perturbations were demonstrated by simulating MAVRIC images in the presence of computed B_0 and B_1 magnetic fields near simple hardware geometries. Both the MAVRIC and SEPI-VAT techniques image under the CPMG condition, which was assumed in all simulated images. B_0 fields were computed using a rapid computational mechanism that was previously demonstrated capable of accurately predicting B_0 distributions induced by metal implants [4]. B_1 magnetic fields were computed using finite element methods (COMSOL Multiphysics®). MAVRIC images were simulated using 35 1kHz spectral bins, 1mm x 2mm x 3mm respective resolutions in the frequency and 2 phase-encoded dimensions, 256 samples collected at +/125 kHz readout bandwidths (1 ms readout), and 2.25 kHz FWHM Gaussian spectral responses. Empirical MAVRIC images were collected at the same settings.

Frequency encoding limitations were effectively simulated by assigning 5 spin isochromats to each encoded pixel in the readout dimension. Spectral dispersion effects during the readout were estimated by assuming linear through-voxel dispersion in the 2 phase-encoded dimensions. An analytic sinc solution for signal truncation due to such linear phase dispersion [5] was then applied during the readout simulation. B_1-induced signal modulation was applied in image space under an assumption of low flip angle RF refocusing (valid for the 135° refocusing pulses utilized in the MAVRIC method).

A metal implant phantom was devised of a Cobalt-Chromium (CoCr) femoral head component from a total hip replacement affixed to a cylindrical titanium shaft. To assess B_1 modulations in the absence of significant induced B_0 gradients, a plastic sphere covered in copper foil was mounted to a plastic post.

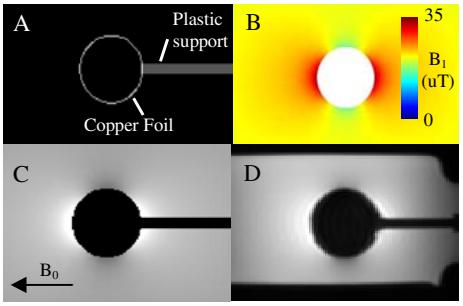

Fig 1: A) Phantom and simulation model used for demonstration of B_1 effects. B) Simulated B_1 perturbation field (B_1+ =B_1- due to azimuthal symmetry). C) Simulated MAVRIC image, and D) measured MAVRIC image

Results and Discussion

Figure 1 demonstrates the effect of B_1 perturbations on MAVRIC images without the presence of significant B_0 effects. Fig 1A depicts the structure of the B_1 investigation phantom, a 4.4 cm diameter sphere coated in copper foil affixed to a plastic support rod. The impact of the computed B_1 distribution (B) on the simulated MAVRIC image (C) clearly correlates with the empirically measured image (D). The intensity changes track similarly in the simulated and measured images, with a signal increase of up to 60% and a signal decrease of up to 40%.

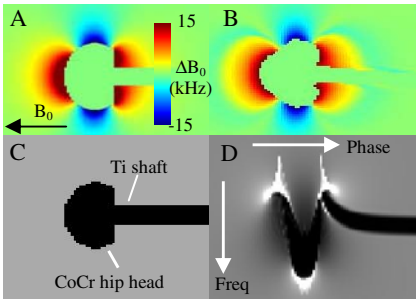

Fig 2: A) Computed and (B) measured B_0 distributions around CoCr and titanium implant assembly. (C) Input magnetization distribution for simulation indicating implant components. (D) Simulation of image using no RF limitations (infinite RF bandwidth). Frequency and phase-encoded dimensions are indicated and utilized for all other simulations

Fig 2 shows computed (A) and empirical (B) B_0 field maps induced by the metal implant phantom. Though the two maps clearly demonstrate similar features, the spatial extent of the MAVRIC-based (B) field map is limited by the artifacts under study in this work. Fig 2C displays the input model for simulation and (D) presents a simulated image whereby no spectral sub-binning is applied (i.e assuming the use of RF pulses that span the entire spectrum induced by the implant, ~30 kHz). The artifacts in this image are similar in magnitude to those encountered when conventional slice-selective imaging is applied near such implants. Directions of frequency and phase-encoding are indicated in Fig. 2 D.

Figure 3 presents simulated (A) and empirical (B) MAVRIC images, where the simulated image does not yet include the effects of B_1 perturbations. There is general agreement between the empirical and simulated images in the approximate locations of intensity increases and decreases. The areas of intensity increase correlate with regions where the induced B_0 gradient in the readout direction (Fig 3C) is nearly equal in magnitude and opposite in polarity to the applied readout gradient. This effectively destroys the spatial encoding process and results in a non-selective integration of signal in the frequency-encoded dimension at these locations. Areas of signal reduction are due to 1) local gradients in the frequency-encoded dimension decreasing the effective encoding to sub-voxel dimensions and 2) through-voxel gradients in the phase-encoded dimensions (Fig 3D) dispersing phase throughout the temporal readout.

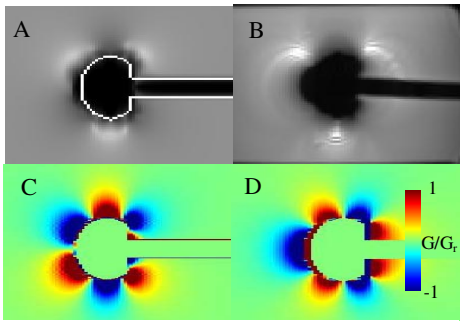

Fig 3: A) Simulated (no B_1 perturbations) and empirical (B) MAVRIC images. C) Induced B_0 gradient in the frequency encoded dimension. D) Induced B_0 gradient in the phase-encoded dimension. Gradients are displayed as a ratio of the utilized frequency-encoding gradient (G_r~33 mT/m).

Figure 4 adds in the effect of B_1 perturbations (A) to the metal implant simulation (B). While the added effect is subtle in comparison to the B_0 gradient effects, there is clearly some impact in the resulting final image intensity, which results in yet further agreement with the intensity variations in the empirical MAVRIC image in Figure 3B. The specific geometric shapes of the intensity artifacts are not identically replicated in the simulation, which is a suspected result of imperfections in the utilized implant model. In particular, a truncated spherical dome geometry was assumed in the simulation model, while the actual implant has a more complicated surface curvature.

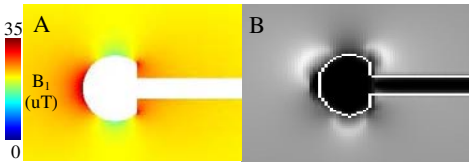

Fig 4: A) Computed B_1+ field around the metal implant assembly. B) Simulated MAVRIC image with the additional consideration of B_1 perturbations.

These results successfully demonstrate and explain the current physical limitations encountered when imaging directly adjacent to metal implants. Though recently developed methods such as MAVRIC and SEPI-VAT dramatically improve spatial encoding capabilities near metal implants (i.e. compared to Fig. 2D), severe B_0 gradients can limit the inherent capabilities of Fourier-based frequency encoding. To a lesser extent, B_1 perturbations also impede any (non-Adiabatic) imaging attempts in the immediate vicinity of implants. From the simulations and results in the present work, it can be estimated that signal within 3-5 mm of Cobalt-Chromium implant interfaces could suffer significant frequency encoding challenges. .

References: 1. Koch et al, ISMRM 2008, p1250. 2. Koch et al, MRM, in press, 3. Lu et al, ISMRM 2008, p838, 4. Koch and Hinks, ISMRM 2008, p 1180, 5. Y. Zhao et al , JMR. 173 2005 10–22.